the energy of the $m_f = -7/2$ cloud is more clear (Fig. 3b). We compare the position of this energy threshold to the expected atom–atom transition frequency ν_{atom} based upon a calibration of the magnetic field strength. The data are consistent with a theoretical calculation of the binding energy (solid line) based upon a full coupled channels calculation with no free parameters.

This agreement with theory leaves no doubt that we are creating large numbers of weakly bound molecules. These highly vibrationally excited molecules could be used to study ultracold molecule–molecule, or molecule–atom, collisions[22,24,25]. Further, the explicit coupling of a quantum degenerate gas of fermionic atoms to bosonic molecules could possibly be developed as a method to facilitate creation of a predicted exotic fermionic superfluid. In addition, our molecule detection technique could be extended to measure the gap energy in this superfluid phase[26,27]. □

Received 29 April; accepted 19 May 2003; doi:10.1038/nature01738.

1. Wynar, R., Freeland, R. S., Han, D. J., Ryu, C. & Heinzen, D. J. Molecules in a Bose-Einstein condensate. *Science* **287,** 1016–1019 (2002).
2. Donley, E. A., Claussen, N. R., Thompson, S. T. & Wieman, C. E. Atom–molecule coherence in a Bose–Einstein condensate. *Nature* **417,** 529–533 (2002).
3. Holland, M., Kokkelmans, S. J. J. M. F., Chiofalo, M. L. & Walser, R. Resonance superfluidity in a quantum degenerate Fermi gas. *Phys Rev. Lett.* **87,** 120406 (2001).
4. Timmermans, E., Furuya, K., Milloni, P. W. & Kerman, A. K. Prospect of creating a composite Fermi-Bose superfluid. *Phys. Lett. A* **285,** 228–233 (2001).
5. Feshbach, H. A unified theory of nuclear reactions. *II. Ann. Phys. (NY)* **19,** 287–313 (1962).
6. Stwalley, W. C. Stability of spin-aligned hydrogen at low temperatures and high magnetic fields: New field-dependent scattering resonances and predissociations. *Phys. Rev. Lett.* **37,** 1628–1631 (1976).
7. Tiesinga, E., Verhaar, B. J. & Stoof, H. T. C. Threshold and resonance phenomena in ultracold ground-state collisions. *Phys. Rev. A* **47,** 4114–4122 (1993).
8. Inouye, S. *et al.* Observation of Feshbach resonances in a Bose–Einstein condensate. *Nature* **392,** 151–154 (1998).
9. Cornish, S. L., Claussen, N. R., Roberts, J. L., Cornell, E. A. & Wieman, C. E. Stable ^{85}Rb Bose-Einstein condensates with widely tunable interactions. *Phys. Rev. Lett.* **85,** 1795–1798 (2000).
10. Loftus, T., Regal, C. A., Ticknor, C., Bohn, J. L. & Jin, D. S. Resonance control of elastic collisions in an optically trapped Fermi gas of atoms. *Phys. Rev. Lett.* **88,** 173201 (2002).
11. Dieckmann, K. *et al.* Decay of an ultracold fermionic lithium gas near a Feshbach resonance. *Phys. Rev. Lett.* **89,** 203201 (2002).
12. O'Hara, K. M. *et al.* Measurement of the zero crossing in a Feshbach resonance of fermionic ^{6}Li. *Phys. Rev. A* **66,** 041401 (2002).
13. Regal, C. A., Ticknor, C., Bohn, J. L. & Jin, D. S. Tuning p-wave interactions in an ultracold Fermi gas of atoms. *Phys. Rev. Lett.* **90,** 053201 (2003).
14. O'Hara, K. M., Hemmer, S. L., Gehm, M. E., Granade, S. R. & Thomas, J. E. Observation of a strongly interacting degenerate Fermi gas of atoms. *Science* **298,** 2179–2182 (2002).
15. Regal, C. A. & Jin, D. S. Measurement of positive and negative scattering lengths in a Fermi gas of atoms. *Phys. Rev. Lett.* (in the press).
16. Bourdel, T. *et al.* Measurement of interactions energy near a Feshbach resonance in a ^{6}Li Fermi gas. Preprint at ⟨http://arXiv.org/cond-mat/0303079⟩ (2003).
17. Timmermans, E., Tommasini, P., Hussein, M. & Kerman, A. Feshbach resonances in atomic Bose-Einstein condensates. *Phys. Rep.* **315,** 199–230 (1999).
18. Abeelen, F. A. & Verhaar, B. J. Time-dependent Feshbach resonance scattering and anomalous decay of a Na Bose-Einstein condensate. *Phys. Rev. Lett.* **83,** 1550–1553 (1999).
19. Mies, F. H., Tiesinga, E. & Julienne, P. S. Manipulation of Feshbach resonance in ultracold atomic collisions using time-dependent magnetic fields. *Phys. Rev. A* **61,** 022721 (2000).
20. Stenger, J. *et al.* Strongly enhanced inelastic collisions in a Bose-Einstein condensate near Feshbach resonances. *Phys. Rev. Lett.* **82,** 2422–2425 (1999).
21. DeMarco, B. & Jin, D. S. Onset of Fermi degeneracy in a trapped atomic gas. *Science* **285,** 1703–1706 (1999).
22. Soldán, P., Cvitas, M. T., Hutson, J. M., Honvault, P. & Launay, J.-M. Quantum dynamics of ultracold Na + Na_2 collisions. *Phys. Rev. Lett.* **89,** 153201 (2002).
23. Ratcliff, L. B., Fish, J. L. & Konowalow, D. D. Electronic transition dipole moment functions for transitions among the twenty-six lowest-lying states of Li_2. *J. Mol. Spectrosc.* **122,** 293–312 (1987).
24. Balakrishnan, N., Forrey, R. C. & Dalgarno, A. Quenching of H_2 vibrations in ultracold ^{3}He and ^{4}He collisions. *Phys. Rev. Lett.* **80,** 3224–3227 (1998).
25. Forrey, R. C., Balakrisnan, N., Dalgarno, A., Haggerty, M. R. & Heller, E. J. Quasiresonant energy transfer in ultracold atom-diatom collisions. *Phys. Rev. Lett.* **82,** 2657–2660 (1999).
26. Petrosyan, K. G. Fermionic atom laser. *JETP Lett.* **70,** 11–16 (1999).
27. Torma, P. & Zoller, P. Laser probing of atomic Cooper pairs. *Phys. Rev. Lett.* **85,** 487–490 (2000).

Acknowledgements We thank E. A. Cornell, C. E. Wieman, C. H. Greene and S. Inouye for discussions. This work was supported by the NSF and NIST; C.A.R. acknowledges support from the Hertz Foundation.

Competing interests statement The authors declare that they have no competing financial interests.

Correspondence and requests for materials should be addressed to C.A.R. (regal@jilau1.colorado.edu).

Achromatic Fresnel optics for wideband extreme-ultraviolet and X-ray imaging

Yuxin Wang*, Wenbing Yun* & Chris Jacobsen*†

** Xradia, Inc., 4075A Sprig Drive, Concord, California 94520, USA*
† Department of Physics & Astronomy, Stony Brook University, Stony Brook, New York 11794, USA

Advances in extreme-ultraviolet (EUV) and X-ray optics are providing powerful new capabilities in high-resolution imaging and trace-element analysis of microscopic specimens[1], and the potential for fabricating devices of smaller critical dimensions in next-generation integrated circuit lithography[2]. However, achieving the highest resolution with such optics usually requires the illuminating EUV or X-ray beam to be highly monochromatic. It would therefore be highly desirable to have large-field-of-view, sub-100-nm resolution optics that are achromatic to a significant degree, allowing more light to be utilized from broader bandwidth sources such as laser-produced plasmas. Here we report an achromatic Fresnel optical system for EUV or X-ray radiation that combines a Fresnel zone plate with a refractive lens with opposite chromatic aberration. We use the large anomalous dispersion property of the refractive lens material near an absorption edge to make its fabrication practical. The resulting structure can deliver a resolution comparable to that of the Fresnel zone plates that have achieved the highest resolution (25 nm; ref. 3) in the entire electromagnetic spectrum, but with an improvement of two or more orders of magnitude in spectral bandwidth.

When Röntgen discovered X-rays in 1895, he immediately searched for a means to focus them[4,5]. On the basis of uncertain observations of slight refraction in prisms, he stated that the index of refraction for X-rays in materials must be no more than about $n = 1.05$ if it differed at all from unity. Two decades later, Einstein[6] proposed that the refractive index for X-rays was $n = 1 - \delta$ with $\delta \approx 10^{-6}$, allowing for total external reflection at grazing incidence angles satisfying $\cos\theta_c = 1 - \delta$, giving $\theta_c \approx \sqrt{2\delta}$ or of the order of 1 mrad (here θ_c is the critical angle). Modern measurements give critical angles of, for example, 9 mrad for 8.98-keV X-rays from gold surfaces; nonetheless, this sets a fundamental limit to the maximum numerical aperture, NA (and thus spatial resolution), of polychromatic X-ray focusing optics. While these optics have advanced from early demonstrations[7] to sub-500-nm focusing[8], demonstrated routes to higher spatial resolution EUV and X-ray imaging and lithography have instead involved optics for monochromatic radiation. Such optics include Fresnel zone plates[9] with 25-nm potential image resolution[3] and high efficiency; simple[10], Fresnel[11], and compound[12] refractive lenses with spatial resolution to about 200 nm (ref. 13); and mirror optics coated with synthetic multilayers[14] which have achieved 50-nm resolution in lithography applications[15]. These approaches have led to significant advances in EUV and X-ray science.

However, all of these higher-resolution methods require the illuminating EUV or X-ray beam to be highly monochromatic. For certain experiments, such as absorption spectroscopy with focused, monochromatized X-ray beams, the demands of these optics for narrow spectral bandwidth illumination are easily met without compromising experimental throughput. With broader-bandwidth EUV or X-ray sources, such as laser-produced plasmas and line emission from X-ray targets, the availability of achromatic optics would allow significantly more light to be utilized for experiments and applications.

The achromatic Fresnel objective combines a high-spatial-resolution Fresnel zone plate with a refractive lens operating in the anomalous dispersion condition to achieve these desirable properties. We begin by considering the properties of Fresnel zone plates. These optics make use of a series of concentric absorbing or phase-shifting rings with prescribed radii, giving a focal length of

$$f_Z = \frac{R^2}{\lambda N} = \frac{2R\Delta R}{\lambda} \tag{1}$$

where $2R$ is the diameter of the optic, ΔR is the width of the finest, outermost zone of zone number N, and λ is the wavelength. For imaging at the Rayleigh limit of 0.61λ/NA, the spatial resolution is $1.22\Delta R$. The number of zones N determines the required illumination monochromaticity or spectral bandwidth:

$$\frac{N}{2} = \frac{R}{4\Delta R} = \frac{\lambda}{\Delta\lambda} \tag{2}$$

Combining these requirements, we see that if we wish to have a large diameter $2R$ for a large field of view and long focal length, large values of N and thus narrow bandpass $\Delta\lambda/\lambda = 2/N$ radiation is required. For example, a zone plate with a diameter of a few millimetres and <100-nm outer zone width would have over 10,000 zones, and therefore a frequently impractical 0.01% bandwidth.

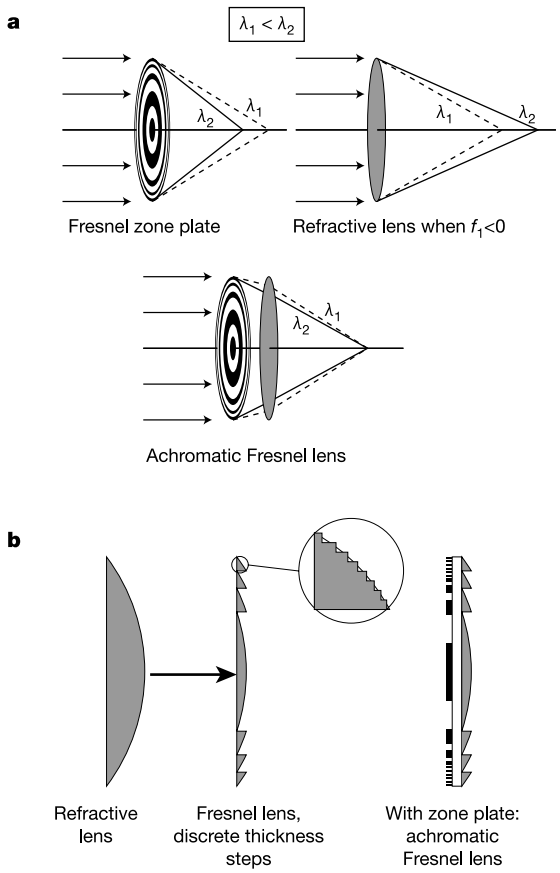

Figure 1 The principle of an achromatic Fresnel lens, and an example of how it can be realized in a single optic. The chromatic aberrations of a zone plate produce a longer focal length for shorter wavelengths (λ_1) than for longer wavelengths (λ_2) (**a**). The chromatic aberrations of a refractive lens are opposite; **a** shows a convex refractive lens for wavelength regions where f_1 is decreasing as the wavelength λ is decreased. One can thus combine the two optic types to cancel chromatic aberration over a certain wavelength range. The simplest such combination (**b**) involves fabrication of a zone plate and a plano-convex refractive lens on opposite sides of a single window; one can also replace the refractive lens with a refractive Fresnel lens to minimize absorption, and also use a staircase approximation to the curvature of the refractive Fresnel lens surface.

We now consider refractive lenses. For a thin lens with a single curved surface of radius R_C, the focal length is given by

$$f_R = \frac{R_C}{n-1} \tag{3}$$

where n is the refractive index of the material. At wavelengths shorter than about 50 nm, the refractive index has the form

$$n = 1 - (\delta + i\beta) = 1 - \alpha\lambda^2(f_1 + if_2) \tag{4}$$

where $\alpha = n_a r_e/2\pi$. In this expression, n_a is the number of atoms per volume, $r_e = 2.8 \times 10^{-15}$ m is the classical radius of the electron, and $(f_1 + if_2)$ is the complex number of effective electrons per atom[16]. Ignoring the absorptive part f_2 of the refractive index, we see that the focal length of a refractive lens for EUV and X-ray radiation is given by

$$f_R = \frac{R_C}{-\alpha\lambda^2 f_1} \tag{5}$$

so that a concave lens produces positive focusing when $f_1 > 0$, the opposite of the usual case for visible light.

A refractive lens is strongly chromatic, as its focal length scales as the inverse of λ^2 and $f_1(\lambda)$. Moreover, its focal length is too weak to be used as a single focusing optic because the quantity $\alpha\lambda^2 f_1$ has the value of 10^{-3} to 10^{-6} for EUV light and X-rays, as anticipated by Einstein. It is only with 'hard' X-rays of energy greater than about 5 keV, where absorption is less problematic, that multiple weak refractive lenses can be stacked up into a compound refractive X-ray lens[12]. The image resolution at present achieved is in the 300-nm range, being limited by absorption, imperfections in the fabrication of the refracting thickness profile, and alignment and depth of focus effects[13].

The achromatic Fresnel optic combines these two optics to cancel the chromatic aberration over a reasonable wavelength range (Fig. 1; other combinations of diffractive and refractive optics have been used to obtain different chromatic effects[17], and zone plate achromatic doublets have also been proposed[18]). Let us consider the imaging properties of each lens as the wavelength is varied from a reference value λ as $\lambda + \Delta\lambda$. The focal length of a Fresnel zone plate is then given by:

$$f_{Z'} \approx f_Z \frac{1}{1 + \frac{\Delta\lambda}{\lambda}} \tag{6}$$

With the refractive lens, we must consider the variation both in $\lambda^2 \rightarrow \lambda^2 + 2\lambda\Delta\lambda + (\Delta\lambda)^2$, and also in f_1. It is well known that the real part of the refractive index f_1 can have a strong dependence on wavelength near an absorption resonance owing to anomalous dispersion. This effect is also exploited in multiple-wavelength anomalous dispersion (MAD) methods in protein crystallography[19]. The simplest approximation that we can make to f_1 is to incorporate a linear dispersive term and write it as:

$$f_1 \rightarrow f_1 + \frac{\Delta f_1}{\Delta\lambda}\Delta\lambda \tag{7}$$

Ignoring terms of order $[\Delta\lambda/\lambda]^2$, the focal length of a refractive lens becomes:

$$f_{R'} \approx f_R \frac{1}{1 + 2\frac{\Delta\lambda}{\lambda} + \frac{\Delta f_1}{f_1}} \tag{8}$$

If the two lenses are placed in close proximity to each other, their reciprocal focal lengths can be added:

$$\frac{1}{f_C} = \frac{1}{f_{Z'}} + \frac{1}{f_{R'}} = \frac{1}{f_Z} + \frac{1}{f_R} + \frac{\Delta\lambda}{\lambda}\left[\frac{1}{f_Z} + \frac{1}{f_R}(2 + D)\right] \tag{9}$$

where $D \equiv (\Delta f_1/f_1)/(\Delta\lambda/\lambda)$ characterizes the dispersion. If the term in the bracket becomes zero, the focal length becomes

independent of $\Delta\lambda$; that is, we have an achromat. Note that one can also seek large values of the bracketed term if it is desired to enhance the chromatic dispersion of a zone plate. The achromat condition can be written as:

$$\frac{f_R}{f_Z} = -(2 + D) \tag{10}$$

The values of f_1 and D can be calculated from absorption data by the Kramers–Kronig relations[16,20], such as are shown in Fig. 2 for the Si and Cu L edges. Near the absorption edges, the magnitude of D can be significantly larger than 2, so that the focal length of the refractive lens is much longer than that of the zone plate (several metres versus several centimetres in our examples). As a result, the refractive lens by itself contributes only weakly to the net focusing action (it is only used as a dispersive corrector), so that the spatial resolution is determined almost solely by the Fresnel zone plate. This long refractive focal length goes along with a larger, easier-to-fabricate radius of curvature for the refractive lens component; this radius of curvature R_C can be written as:

$$R_C \approx \alpha(2R\Delta R)\lambda^2 \frac{\Delta f_1}{\Delta\lambda} \tag{11}$$

Since $(\Delta f_1/\Delta\lambda)$ tends to be largest when it has a positive value near X-ray absorption edges (see Fig. 2), convex or plano-convex solutions for the refractive correction lens are preferred. In addition, the use of wavelengths longer than the absorption edge is preferred for EUV light and soft X-rays to reduce absorption. Finally, we note that the bandwidth gain depends on both the number of zones in the zone plate and on the dispersion properties of the refractive lens material. A schematic illustration of the effect is shown in Fig. 1.

The use of anomalous dispersion increases the radius of curvature and thus minimizes the total thickness of convex refractive lens components. However, at EUV wavelengths in particular the absorption from the thicker lens regions may be unacceptable. One solution is to replace the refractive lens with a refractive Fresnel lens so that the overall curvature can be maintained within a stepwise approximation. Ideally these thickness steps shift the phase of the transmitted light by an integer multiple of 2π. Other thickness steps can be chosen if the resulting phase error is compensated by adjustment of the zone positions of the Fresnel zone plate. It should be noted that an aberration-free Fresnel lens imposes a certain requirement for monochromaticity. As indicated by equation (4), the accumulated phase difference between a wave that propagates a distance t through free space and one that propagates the same distance through a material is $kt\delta$, so that a wavefront is displaced by a distance of $t\delta$. For illumination with a bandwidth of $\Delta\lambda$, the coherence length is given by $\lambda^2/(\Delta\lambda)$, so one must have $t\delta < \lambda^2/(\Delta\lambda)$ or $t < (\lambda/\Delta\lambda)\lambda/\delta$. If we consider the example of Fig. 2 of $\lambda = 13.5$ nm in Si where $\delta = 9.5 \times 10^{-4}$ and

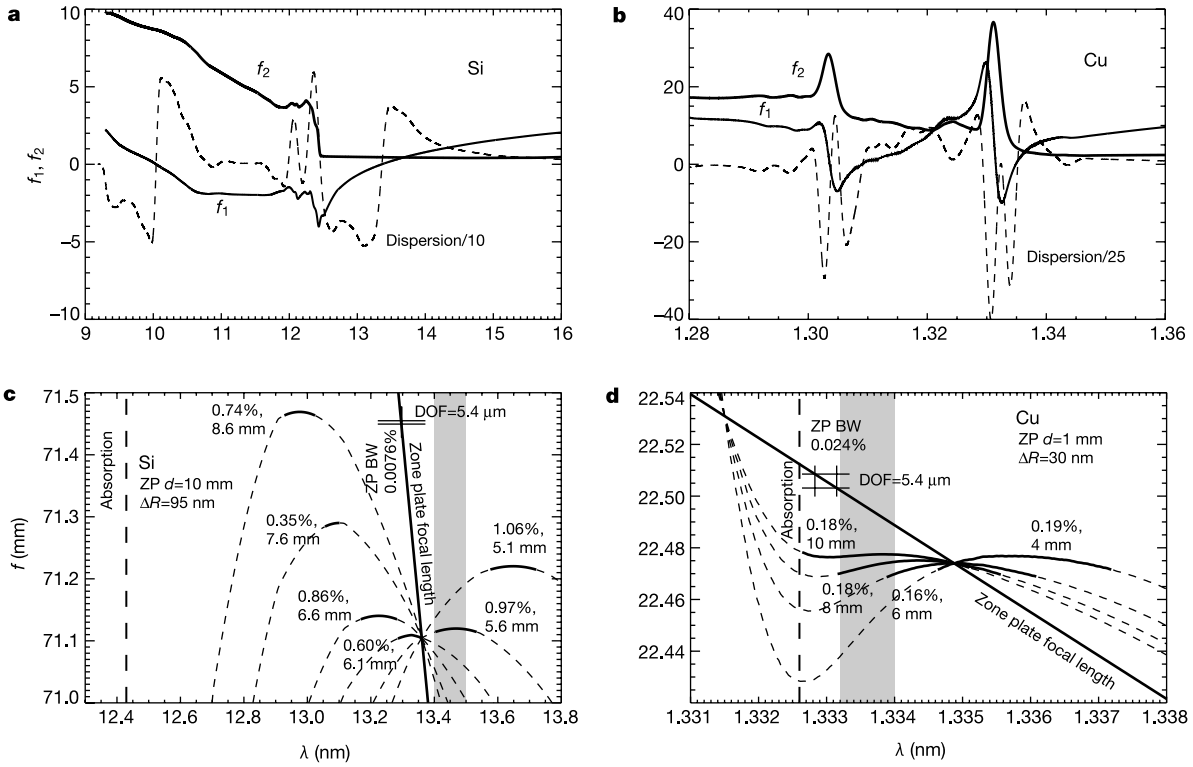

Figure 2 X-ray optical constants and their consequences for EUV and soft X-ray achromatic Fresnel objectives. At top (**a**, **b**) are shown the oscillator strengths ($f_1 + if_2$) and the dispersion D for silicon and copper L edges. The absorptive term f_2 was determined from thin-film absorption measurements Fourier-filtered with a Hanning cut-off of 0.2 eV (Si; from ref. 25) or 0.7 eV (Cu in $SrCuO_2$; from ref. 26). The phase-shifting term f_1 was calculated by inserting the measured near-absorption-edge data into tabulated values for f_2, and then using this data to modify tabulated values of f_1 using the Kramers–Kronig relationship[16]; this procedure was able to reproduce experimental measurements[27] of near-edge f_1 values from near-edge f_2 data of amorphous carbon. At bottom (**c**, **d**) are shown examples of achromatic Fresnel objective configurations at wavelengths longer than the absorption edge of each element. The focal length (f) of a Fresnel zone plate (ZP) changes significantly over the wavelength range shown, especially when compared with the depth of field $2\lambda/(\mathrm{NA})^2$ of the optic, so that only very narrow bandwidth (BW) radiation can be used for imaging. However, when an achromatic Fresnel lens is produced by combining the zone plate with a refractive lens, the combined focal length (for several values of refractive lens radius of curvature R_C) is constant to within a depth of field, DOF (as indicated by thickened lines for the combined focal length), over bandwidths approaching 1% for Si and 0.2% for Cu with these sets of parameters. In **c**, we indicate with a grey band the 13.4–13.5 nm wavelength band used in EUV lithography systems, while in **d** the grey band corresponds to the Cu Lα fluorescence line. Note that improved measurements of absorption spectra and thus f_2 values would lead to refined estimates of achromatic bandwidth. d, diameter of the zone plate.

the allowable achromatic bandwidth is 0.97% or $(\lambda/\Delta\lambda) = 103$, we see that a thickness difference of up to 1.5 mm between the refractive lens and the refractive Fresnel lens profile still satisfies the coherence length requirement for the bandwidth used. It is this net thickness difference that is the important parameter; one could go up to this limit in $(\lambda/\Delta\lambda) = 103$ steps of 2π phase change, or 34 steps of 6π phase change, to pick two examples. Finally, since the radius r of a plano-convex lens with a thickness t at its centre is given by $r = \sqrt{2R_C t - t^2}$, with $R_C = 5.6$ mm and $t = 1.5$ mm one can have a lens radius up to 3.8 mm (or a numerical aperture of up to 0.75) and still remain within the coherence length requirement of a Fresnel lens with 0.93% bandwidth.

In practice, one can imagine lithographically fabricating an achromatic Fresnel optic (AFO) on a single thin membrane, with the Fresnel zone plate fabricated on one side, and a refractive Fresnel lens on the other side, as shown in Fig. 1 (possibly fabricated using multilevel[21,22] or imprint[23] methods). The achievable efficiencies of the zone plate and the Fresnel lens are about 30–50% and 30–80%, respectively, leading to a combined efficiency of 10–40% for the AFO which compares quite favourably with, for example, the ~5% net throughput of a next-generation lithography system using six optics with 60% reflectivity each to gain the required resolution and field of view.

The size of the AFO and its imaging field are likely to be limited by primary aberrations. Seidel wavefront aberrations for imaging finite conjugates with zone plate optics have been calculated by Young[24]. At 1.34-nm wavelength (Cu L absorption edge) with a 4:1 demagnifying geometry (a standard set-up used in lithography cameras), aberration-free imaging fields of between 2 and 15 mm can be expected for outermost zone widths between 40 and 95 nm without aberration correction. When used with EUV radiation near 12.5 nm wavelength, the NAs are increased nearly tenfold and primary aberrations become more problematic unless the field of view is kept to a few tenths of 1 mm. Spherical aberration does not exist for Fresnel zone plates when the zone placement is computed for a specific imaging geometry. This property, along with the achromatic nature of the AFO, allows one to reduce the field curvature and astigmatism to an acceptable level by increasing the AFO diameter (therefore the focal length) while maintaining the same field of view. Coma can be reduced and eliminated in some cases by appropriate aperturing.

In general, the AFO design provides two important benefits: it makes a large bandwidth of electromagnetic radiation usable, and it allows large-diameter high-resolution optics to be produced without suffering from chromatic aberration. The increased bandwidth should greatly improve the throughput of applications using broadband X-ray sources, such as X-ray tubes and laser-produced plasmas. In addition, non-spectroscopic imaging applications such as tomography at synchrotron radiation sources could operate with reduced imaging time using multilayer monochromators rather than narrow-bandpass crystal monochromators. The large diameter gives large working distance and large imaging field, both valuable attributes in imaging applications. The present AFO design has the potential to make significant impact in X-ray microscopy and microanalysis, and next-generation lithography applications. □

Received 27 January; accepted 19 May 2003; doi:10.1038/nature01756.

1. Meyer-Ilse, W., Warwick, T. & Attwood, D. (eds) *X-ray Microscopy: Proceedings of the Sixth International Conference* (American Institute of Physics, Melville, New York, 2000).
2. Chapman, H. N. *et al.* First lithographic results from the extreme ultraviolet engineering test stand. *J. Vac. Sci. Technol. B* **19,** 2389–2395 (2001).
3. Peuker, M. High-efficiency nickel phase zone plates with 20 nm minimum outermost zone width. *Appl. Phys. Lett.* **78,** 2208–2210 (2001).
4. Röntgen, W. C. Über eine neue Art von Strahlen. Vorläufige Mittheilung. *Sber. Phys.-Med. Ges. Würzb.* **137,** 132–141 (1895).
5. Röntgen, W. C. On a new kind of rays. *Nature* **53,** 274–276 (1896).
6. Einstein, A. Lassen sich Brechungsexponenten der Korper für Röntgenstrahlen experimentell ermitteln? *Verh. Dtsch. Phys. Ges.* **20,** 86–87 (1918).
7. Kirkpatrick, P. & Baez, A. V. Formation of optical images by x-rays. *J. Opt. Soc. Am.* **38,** 766–774 (1948).
8. Hignette, O. *et al.* in *X-ray Micro- and Nano-Focusing: Applications and Techniques II* (ed. McNulty, I.) 105–116 (Proc. SPIE, The International Society for Optical Engineering, San Diego, 2001).
9. Baez, A. V. A self-supporting metal Fresnel zone-plate to focus extreme ultra-violet and soft X-rays. *Nature* **186,** 958 (1960).
10. Michette, A. G. *Optical Systems for Soft X-Rays* (Plenum, New York, 1986).
11. Yang, B. X. Fresnel and refractive lenses for X-rays. *Nucl. Instrum. Meth. Phys. Res. A* **328,** 578–587 (1993).
12. Snigirev, A., Kohn, V., Snigireva, I. & Lengeler, B. A compound refractive lens for focusing high energy X-rays. *Nature* **384,** 49–51 (1996).
13. Lengeler, B. *et al.* Parabolic refractive X-ray lenses. *J. Synchrotron Radiat.* **9,** 119–124 (2002).
14. Spiller, E. Low-loss reflection coatings using absorbing materials. *Appl. Phys. Lett.* **20,** 365–367 (1972).
15. Naulleau, P. *et al.* Sub-70-nm EUV lithography at the Advanced Light Source static microfield exposure station using the ETS Set-2 optic. *J. Vac. Sci. Technol. B* **20,** 2829–2833 (2002).
16. Henke, B. L., Gullikson, E. M. & Davis, J. C. X-ray interactions: photoabsorption, scattering, transmission, and reflection at E = 50–30,000 eV, Z = 1–92. *At. Data Nucl. Data Tables* **54,** 181–342 (1993).
17. Dobson, S. L., Sun, P.-C. & Fainman, Y. Diffractive lenses for chromatic confocal imaging. *Appl. Opt.* **36,** 4744–4748 (1997).
18. Michette, A. G., Buckley, C., Gallo, F., Powell, K. & Pfauntsch, S. J. in *Advances in X-ray Optics* (ed. Freund, A. K. *et al.*) 303–310 (Proceedings SPIE Vol. 4145, The International Society for Optical Engineering, Bellingham, Washington, 2000).
19. Hendrickson, W. A. Determination of macromolecular structures from anomalous diffraction of synchrotron radiation. *Science* **254,** 51–58 (1991).
20. Jackson, J. D. *Classical Electrodynamics* (Wiley & Sons, New York, 1975).
21. Stern, M. B. & Medeiros, S. S. Deep three-dimensional microstructure fabrication for infrared binary optics. *J. Vac. Sci. Technol. B* **10,** 2520–2525 (1992).
22. Walsby, E. D. *et al.* Multilevel silicon diffractive optics for terahertz waves. *J. Vac. Sci. Technol. B* **20,** 2780–2783 (2002).
23. Hirai, Y. *et al.* Imprint lithography for curved cross-sectional structure using replicated Ni mold. *J. Vac. Sci. Technol. B* **20,** 2867–2871 (2002).
24. Young, M. Zone plates and their aberrations. *J. Opt. Soc. Am.* **62,** 972–976 (1972).
25. van Buuren, T. W. H. *et al.* Electronic structure of silicon nanocrystals as a function of particle size. *Abstr. Pap. Am. Chem. Soc.* **213,** 313 (1997).
26. Liu, R. S. *et al.* Evidence for electron-doped (*n*-type) superconductivity in the infinite-layer $(Sr_{0.9}La_{0.1})CuO_2$ compound by X-ray absorption near-edge spectroscopy. *Solid State Commun.* **118,** 367–370 (2001).
27. Dambach, S. *et al.* Novel interferometer in the soft x-ray region. *Phys. Rev. Lett.* **80,** 5473–5476 (1998).

Acknowledgements We thank J. Kirz for discussions, and S. Frigo for information about the calculation of Kramers–Kronig transforms.

Competing interests statement The authors declare competing financial interests: see the website (http://www.nature.com) for details.

Correspondence and requests for materials should be addressed to W.Y. (wyun@xradia.com).

Asymmetric pores in a silicon membrane acting as massively parallel brownian ratchets

Sven Matthias & Frank Müller

Max Planck Institute of Microstructure Physics, Weinberg 2, Halle 06120, Germany

The brownian motion of mesoscopic particles is ubiquitous and usually random. But in systems with periodic asymmetric barriers to movement, directed or 'rectified' motion can arise and may even modulate some biological processes[1]. In man-made devices, brownian ratchets and variants based on optical or quantum effects have been exploited to induce directed motion[2–14], and the dependence of the amplitude of motion on particle size has led to the size-dependent separation of biomolecules[6,8,15]. Here we demonstrate that the one-dimensional pores of a macroporous silicon membrane[16], etched to exhibit a periodic asymmetric variation in pore diameter, can act as massively parallel and multiply stacked brownian ratchets that are potentially suitable for large-scale particle separations. We